

Lepton pair production at NNLO in QED with EW effects

Sophie Kollatzsch^{a,b} and Yannick Ulrich^c

^a *Institut für Kern- und Teilchenphysik, TU Dresden, DE-01069 Dresden, Germany*

^b *Paul Scherrer Institut, CH-5232 Villigen PSI, Switzerland*

^c *Institute for Particle Physics Phenomenology, University of Durham,
South Road, Durham DH1 3LE, United Kingdom*

We present a fully differential calculation of lepton pair production, taking into account the dominant next-to-next-to-leading order QED corrections as well as next-to-leading order electroweak, and polarisation effects. We include all lepton masses, hard photon emission, as well as non-perturbative hadronic corrections. The corresponding matrix elements are implemented in the Monte Carlo framework MCMULE. In order to obtain a numerically stable implementation, we extend next-to-soft stabilisation, a universal technique based on a next-to-leading-power expansion, to calculations with polarised leptons. As an example, we show results tailored to the Belle II detector with the current setup as well as a potential future configuration that includes polarised beams.

1 Introduction

Thanks to its high luminosity, Belle II is expected to produce about 45 billion $\tau\tau$ events over its lifetime [1], roughly fifty times more than Belle I [2] and a hundred times more than at BaBar [3]. This increase in statistics will allow for precision measurements of very rare Standard Model (SM) decays such as $\tau \rightarrow \nu\bar{\nu}\ell\ell'$ or $\tau \rightarrow \nu\bar{\nu}\ell\gamma$ as well as put bounds on charged-lepton-flavour-violating decays such as $\tau \rightarrow \ell\ell'\ell'$. For the SM decays, even differential measurements in terms of Michel parameters will be possible. In this case, spin-spin correlations between the two taus of $ee \rightarrow \tau\tau$ can be exploited [4]. Further, it was recently proposed to measure the anomalous magnetic moment of the tau to 10^{-6} by exploiting transverse and longitudinal asymmetries [5].

Hence, the production cross section for $ee \rightarrow \tau\tau$ needs to be known as precisely as possible. For the centre-of-mass (CMS) energy used at Belle II ($\sqrt{s} \approx 10.5$ GeV), QED effects still dominate even though electroweak (EW) effects start to become relevant. With EW effects, we mean all contributions due to EW interactions but without contributions due to pure QED. The Monte Carlo code KKMC [6–8] combines a parton shower with fixed-order EW corrections at next-to-leading order (NLO). It has been very useful for many experimental studies [1]. The EW effects were further studied with the SANC program, accounting for the polarisation of the incoming leptons [9].

However, the improvements expected from Belle II warrant a renewed theoretical effort. Currently no NNLO-QED calculation for $ee \rightarrow \ell\ell$ (with $\ell \neq e$) exists as the necessary two-loop integrals are not currently known with full mass dependence. However, a recent theoretical interest in $e\text{-}\mu$ scattering [10] was inspired by the MUonE experiment [11–13]. As part of this effort, the necessary integrals were computed in the limit of vanishing electron mass $m_e \rightarrow 0$ [14, 15]. This was very recently used to assemble to the full two-loop matrix element (squared) for $ee \rightarrow \ell\ell$ with $m_e = 0$ [16]. Assuming m_e is small compared to all other scales of the process, this matrix element can be used to obtain the full matrix element up to terms suppressed by $\mathcal{O}(m^2/Q^2)$. This *massification* procedure was first developed in [17–19] and later extended [20] to the case of a second, heavy mass.

However, the smallness of the electron mass means, that for a first estimate of the NNLO correction, it is sufficient to just consider the electronic corrections, i.e. those due to the electron, and ignoring the more complicated mixed contributions. This can be done in a gauge-invariant manner by assigning different charges for each lepton family and only take contributions proportional to $Q_\ell^2 Q_e^6$. This was demonstrated at NLO [21] and then exploited to calculate the dominant NNLO contributions to $e\mu \rightarrow e\mu$ [22, 23].

In this paper, we use the MCMULE framework to extend our previous calculation [22] to cover the electronic, or initial-state-radiation (ISR), corrections to $ee \rightarrow \ell\ell$. We further treat the incoming electrons as polarised and include NLO-EW effects that are becoming relevant at the energy at which Belle II operates.

Since the CMS energy of Belle II ($\sqrt{s} \approx 10.5$ GeV) is significantly higher than for MUonE ($\sqrt{s} \approx 0.4$ GeV), new numerical problems arise in the real-virtual matrix element, especially in the case of soft emission. These can be efficiently handled using next-to-soft (NTS) stabilisation [24], i.e. using a next-to-leading power (NLP) expansion if the emitted photon becomes soft.

This paper is organised as follows: in Section 2, we briefly summarise the calculation as implemented in the MCMULE framework. Next, we explain how NTS stabilisation changes when considering polarised particles in Section 3. Finally, we present some results for tau production cross sections and asymmetries, both in general and tailored to Belle II in Section 4 before concluding in Section 5.

2 Overview of the calculation

We consider the scattering process

$$e^+(p_1)e^-(p_2) \rightarrow Z/\gamma \rightarrow \tau^+(p_3)\tau^-(p_4)\{\gamma(p_5)\gamma(p_6)\}, \quad (1)$$

taking into account the full NLO-EW corrections and the electronic NNLO-QED corrections. Since we are well below the Z peak, we expand the NLO-EW corrections in $1/M_Z$ and only retain terms $\mathcal{O}(M_Z^{-2})$. However, we retain full dependence on the electron and tau masses.

Diagrams were generated with FeynArts [25] and QGraf [26] and calculated using Package-X [27]. Ultra-violet (UV) and infrared (IR) divergences are regularised in $d = 4 - 2\epsilon$ dimensions and the renormalisation is performed in the on-shell scheme. For the EW corrections, this means that we would like to use e , M_W , M_Z , and m_ℓ as input parameters [28, 29]. However, it is beneficial to use G_F instead of M_W as it has much higher precision¹

$$\begin{aligned} \alpha &= \frac{e^2}{4\pi} = \frac{1}{137.035999084}, \\ G_F &= 1.1663787 \times 10^{-11} \text{ MeV}^{-2}, \\ M_Z &= 91\,187.6 \text{ MeV}, \\ m_e &= 0.510998950 \text{ MeV}, \\ m_\tau &= 1\,776.86 \text{ MeV}. \end{aligned} \quad (2)$$

The calculation is split into fermionic contributions that are due to vacuum polarisation (VP) effects (Section 2.1) and bosonic ones (Section 2.2). The former can be further split into leptonic contributions (electrons, muons, and taus) and non-perturbative hadronic effects (HVP).

Once properly renormalised, all matrix elements were implemented in version v0.4.0 of the publicly available parton-level integrator MCMULE [22, 30, 31]

<https://mule-tools.gitlab.io>

It performs the phase-space integration using the FKS ^{ℓ} subtraction scheme [32], an all-orders QED extension of the FKS scheme [33, 34]. This allows us to calculate any IR-safe observable in a fully differential way.

Our calculation is performed with longitudinally polarised electrons (see for example [35, 36]). We introduce a polarisation vector n_i along the beam direction for each particle that takes the form

$$\begin{aligned} n_i &= (0, 0, 0, P_i) \\ p_i &= (m_i, 0, 0, 0) \end{aligned} \quad (3)$$

in the particle's rest frame. Of course $n_i \cdot p_i = 0$ in any frame. $|P_i| \leq 1$ is the degree of polarisation that can be chosen as required by the beam parameters. To implement this, we modify the completeness relation of the spinors to

$$u(p_i)\bar{u}(p_i) = (\not{p}_i + m_i)(1 + \not{n}_i\gamma_5). \quad (4)$$

¹The way MCMULE is structured, we actually use M_Z and $s_W^2 = 0.226202$ as variables. However, M_W , and thus s_W , are obtained from G_F .

Alternatively, it may be simpler to calculate the matrix element for fully polarised initial states, i.e. with $P_i \equiv s_i = \pm 1$

$$\mathcal{M}^{s_1 s_2} = |\mathcal{A}|_{P_1=s_1, P_2=s_2}^2. \quad (5)$$

This is for example done in OpenLoops [37, 38] which we will be using in Section 2.2. However, for most phenomenological applications we are interested in partial polarisation. For the (parity conserving) QED part, we can recover the general result as

$$\mathcal{M} = \frac{1 + P_1 P_2}{2} \mathcal{M}^{\pm\pm} + \frac{1 - P_1 P_2}{2} \mathcal{M}^{\pm\mp}, \quad (6)$$

where $-1 \leq P_i \leq +1$ can be arbitrary.

2.1 Fermionic corrections

Up to NNLO, all fermionic corrections to our process are due to closed fermion bubbles. At one-loop, these can be written in terms of the photonic and Z currents for the flavour $f = e, \tau$

$$j_\mu^{(f, \gamma)} = e \bar{v}(p, m_f) \gamma_\mu u(p', m_f), \quad (7a)$$

$$j_\mu^{(f, Z)} = e \bar{v}(p, m_f) \gamma_\mu (g_- P_L + g_+ P_R) u(p', m_f), \quad (7b)$$

with the momenta properly chosen. The $(Z\ell\bar{\ell})$ -couplings are flavour-universal

$$g_- = -\frac{\frac{1}{2} - s_W^2}{s_W c_W} \quad \text{and} \quad g_+ = \frac{s_W}{c_W}. \quad (8)$$

The (renormalised) one-loop amplitude can be divided into three parts

$$\begin{aligned} \mathcal{A}_{\text{vp}}^{(1)} &= \text{Diagram 1} + \text{Diagram 2} + \text{Diagram 3} \\ &+ \text{Diagram 4} + \mathcal{O}\left(\frac{1}{M_Z^4}\right) \\ &= \mathcal{A}_{\text{vp}, \gamma\gamma}^{(1)} + \mathcal{A}_{\text{vp}, \gamma Z}^{(1)} + \mathcal{A}_{\text{vp}, ZZ}^{(1)} + \mathcal{O}\left(\frac{1}{M_Z^4}\right) \\ &= \frac{1}{s^2} j_\mu^{(e, \gamma)} j_\mu^{(\tau, \gamma)} \Sigma_{\gamma\gamma}^{\text{renorm.}}(s) + \frac{1}{s(s - M_Z^2)} \left(j_\mu^{(e, Z)} j_\mu^{(\tau, \gamma)} + j_\mu^{(e, \gamma)} j_\mu^{(\tau, Z)} \right) \Sigma_{\gamma Z}^{\text{renorm.}}(s) \\ &+ \left(\frac{1}{s - M_Z^2} \right)^2 j_\mu^{(e, Z)} j_\mu^{(\tau, Z)} \Sigma_{ZZ}^{\text{renorm.}}(s) + \mathcal{O}\left(\frac{1}{M_Z^4}\right), \end{aligned} \quad (9)$$

where the transversal self-energies $\Sigma_{ij}^{\text{renorm.}}$ are renormalised in the on-shell scheme with the conditions [29]

$$\Sigma_{\gamma\gamma}^{\text{renorm.}}(0) = 0, \quad \text{Re}\left[\Sigma_{ZZ}^{\text{renorm.}}(M_Z^2)\right] = 0, \quad \Sigma_{\gamma Z}^{\text{renorm.}}(0) = 0, \quad \text{Re}\left[\Sigma_{\gamma Z}^{\text{renorm.}}(M_Z^2)\right] = 0. \quad (10)$$

Fermionic contributions due to other particles in the EW sector (such as the Higgs) are suppressed by at least $\mathcal{O}(1/M_Z^4)$ and hence already dropped. For the ZZ term, we extract the part that is $\mathcal{O}(1/M_Z^2)$ by defining a constant C

$$\mathcal{A}_{\text{vp}, ZZ}^{(1)} = \frac{1}{M_Z^2} j_\mu^{(e, Z)} j_\mu^{(\tau, Z)} C + \mathcal{O}\left(\frac{1}{M_Z^4}\right) \quad (11)$$

that arises from the renormalisation of M_Z . Hence, it is determined through the (unrenormalised) self-energy $\Sigma_{ZZ}(Q^2)$ at $Q^2 = M_Z^2$ where it can be calculated perturbatively as it has no kinematic dependence

$$C = \frac{\alpha}{6\pi} \sum_f \frac{(I_3^f)^2 - 2s_W^2 I_3^f Q_f + 2s_W^4 Q_f^2}{c_W^2 s_W^2}. \quad (12)$$

From the renormalisation conditions (10) we also find the explicit expressions for the renormalised self-energies [39]

$$\begin{aligned}\Sigma_{\gamma\gamma}^{\text{renorm.}}(s) &= \Sigma_{\gamma\gamma}(s) - \Sigma_{\gamma\gamma}(0), \\ \Sigma_{\gamma Z}^{\text{renorm.}}(s) &= \text{Re}\left[\Sigma_{\gamma Z}(s)\right] - \Sigma_{\gamma Z}(0) - \frac{s}{M_Z^2}\left(\text{Re}\left[\Sigma_{\gamma Z}(M_Z^2)\right] - \Sigma_{\gamma Z}(0)\right).\end{aligned}\quad (13)$$

By defining the VP function $\hat{\Pi}_{ij}$ [39, 40]

$$\Sigma_{ij}(Q^2) \equiv \Sigma_{ij}(0) + Q^2 \hat{\Pi}_{ij}(Q^2), \quad (14)$$

the $\gamma\gamma$ and γZ amplitudes can be written as

$$\begin{aligned}\mathcal{A}_{\text{vp},\gamma\gamma}^{(1)} + \mathcal{A}_{\text{vp},\gamma Z}^{(1)} \\ = \frac{1}{s} j_\mu^{(e,\gamma)} j_\mu^{(\tau,\gamma)} \hat{\Pi}_{\gamma\gamma}(s) + \frac{1}{(s - M_Z^2)} \left(j_\mu^{(e,Z)} j_\mu^{(\tau,\gamma)} + j_\mu^{(e,\gamma)} j_\mu^{(\tau,Z)} \right) \left(\text{Re}\left[\hat{\Pi}_{\gamma Z}(s)\right] - \text{Re}\left[\hat{\Pi}_{\gamma Z}(M_Z^2)\right] \right).\end{aligned}\quad (15)$$

Using the definitions of `alphaQED` [40]

$$\hat{\Pi}_{\gamma Z}(Q^2) = \frac{1}{s_W c_W} \left(\hat{\Pi}_{3\gamma}(Q^2) - s_W^2 \hat{\Pi}_{\gamma\gamma}(Q^2) \right), \quad (16)$$

where the 3 refers to the third component of the isospin current and γ to the QED current, we arrive at the final expression

$$\begin{aligned}\mathcal{A}_{\text{vp}}^{(1)} &= \frac{1}{s} j_\mu^{(e,\gamma)} j_\mu^{(\tau,\gamma)} \hat{\Pi}_{\gamma\gamma}(s) \\ &\quad - \frac{1}{M_Z^2} \left(j_\mu^{(e,Z)} j_\mu^{(\tau,\gamma)} + j_\mu^{(e,\gamma)} j_\mu^{(\tau,Z)} \right) \text{Re} \left[\frac{1}{s_W c_W} \left(\hat{\Pi}_{3\gamma}(s) - \hat{\Pi}_{3\gamma}(M_Z^2) \right) - \frac{s_W}{c_W} \left(\hat{\Pi}_{\gamma\gamma}(s) - \hat{\Pi}_{\gamma\gamma}(M_Z^2) \right) \right] \\ &\quad + \frac{1}{M_Z^2} j_\mu^{(e,Z)} j_\mu^{(\tau,Z)} C + \mathcal{O}\left(\frac{1}{M_Z^4}\right).\end{aligned}\quad (17)$$

Here, all non-perturbative $\hat{\Pi}_{ij}$ (including $\hat{\Pi}_{ij}(M_Z^2)$) are taken from `alphaQED` and can be obtained more or less directly from R ratio data. However, $\hat{\Pi}_{3\gamma}$ is sensitive to fermions flavour in a different way than $\hat{\Pi}_{\gamma\gamma}$, necessitating a flavour recombination. The simplest strategy for this is assuming that $\text{SU}(3)_f$ is an exact symmetry which results in $\hat{\Pi}_{3\gamma} = \frac{1}{2} \hat{\Pi}_{\gamma\gamma}$. `alphaQEDc19` uses a more complicated strategy based on vector meson dominance (VMD) [40].

Beyond NLO, we have to account for QED-VP insertions into loop diagrams. This is done using the hyperspherical method [41, 42] that was used for μ - e scattering [43] and implemented in `MCMULE` for μ - e , ℓ - p , and Møller scattering [22, 44].

2.2 Bosonic corrections

At NNLO, we have three separately divergent types of contributions: virtual-virtual (VV), real-virtual (RV), and real-real (RR).

For the electronic corrections, the VV can be obtained from the heavy-quark form factor [45] which is written in terms of harmonic polylogarithms (HPLs) [46]. This allows for trivial analytic continuation into the time-like region we are interested in.

We use `OpenLoops` [37, 38] in its standard mode for the RV corrections. While `OpenLoops` is extremely stable, its standard mode may not be sufficient for soft or collinear emission, especially in the case of small fermion masses. To address this issue, we use NTS stabilisation [24]. The basic idea of this method is to switch to an expanded matrix element if the (rescaled) photon energy $\xi = 2E_\gamma/\sqrt{s}$ drops below a certain cut-off. This cut-off is usually varied between 10^{-5} and 10^{-2} to ensure that the final result does not depend on its value.

Below the cut-off, we use a matrix element that is expanded for small photon energies up to NLP. To do this, we use an extension of the LBK theorem [47, 48] to one loop [49, 50] that we will discuss in the next section.

3 LBK theorem for polarised particles

Following [49, 50], we will extend the LBK theorem to polarised cross sections at one loop. We use ξ as the expansion parameter and write the photon momentum as $p_\gamma = \xi k$.

To better understand what happens at one loop, let us first review the changes in the case of polarised particles in the proof at tree-level where similar results have been obtained before [51, 52]. By splitting $\mathcal{A}_{n+1}^{(0)}$ into contributions from internal and external legs

$$\mathcal{A}_{n+1}^{(0)} = \sum_i \left(\text{Diagram with } \Gamma^{\text{ext}} \text{ and } p_\gamma \text{ on external leg } i \right) + \text{Diagram with } \Gamma^{\text{int}} \text{ and } p_\gamma \text{ on internal leg}, \quad (18)$$

and using gauge invariance, the NTS contribution can be written as [47–50]

$$\mathcal{A}_{n+1}^{(0)} = \sum_i Q_i \left(\frac{1}{\xi} \frac{\epsilon \cdot p_i}{k \cdot p_i} \Gamma^{\text{ext}}(\{p\}) - \frac{\Gamma^{\text{ext}}(\{p\}) \not{k} \not{\epsilon}}{2k \cdot p_i} - [\epsilon \cdot D_i \Gamma^{\text{ext}}(\{p\})] \right) u(p_i) + \mathcal{O}(\xi^1), \quad (19)$$

with the LBK operator

$$D_i^\mu = \frac{p_i^\mu}{k \cdot p_i} k \cdot \frac{\partial}{\partial p_i} - \frac{\partial}{\partial p_{i,\mu}}. \quad (20)$$

When squaring $\mathcal{A}_{n+1}^{(0)}$, we have to consider the interference between the leading-power (LP, $\mathcal{O}(\xi^{-1})$ at amplitude-level) and NLP ($\mathcal{O}(\xi^0)$ at amplitude-level) terms. To do this in the unpolarised case, we would use the identity

$$\frac{u(p_i) \bar{u}(p_i) \not{\epsilon} \not{k} + \not{\epsilon} \not{k} u(p_i) \bar{u}(p_i)}{2k \cdot p_i} = \frac{\epsilon \cdot p_i}{k \cdot p_i} \not{k} - \not{\epsilon} = \epsilon \cdot D_i \left(u(p_i) \bar{u}(p_i) \right) \quad (21)$$

since $u(p_i) \bar{u}(p_i) = \not{p}_i + m_i$. In the polarised case, we have to use (4) and (21) gets modified accordingly

$$\frac{u(p_i) \bar{u}(p_i) \not{\epsilon} \not{k} + \not{\epsilon} \not{k} u(p_i) \bar{u}(p_i)}{2k \cdot p_i} = \left[\epsilon \cdot D_i - \frac{\epsilon_\mu k_\nu - \epsilon_\nu k_\mu}{k \cdot p_i} n_{i,\nu} \frac{\partial}{\partial n_{i,\mu}} \right] \left(u(p_i) \bar{u}(p_i) \right). \quad (22)$$

Hence, the matrix element is finally obtained after summing over the polarisation of the photon

$$\mathcal{M}_{n+1}^{(0)}(\{p\}, k) = \sum_{ij} Q_i Q_j \left(-\frac{1}{\xi^2} \frac{p_i \cdot p_j}{(k \cdot p_i)(k \cdot p_j)} + \frac{1}{\xi} \frac{p_j \cdot D_i}{k \cdot p_j} + \frac{1}{\xi} \frac{p_{j,\mu} k_\nu - p_{j,\nu} k_\mu}{(k \cdot p_i)(k \cdot p_j)} n_{i,\nu} \frac{\partial}{\partial n_{i,\mu}} \right) \mathcal{M}_n^{(0)}(\{p\}) + \mathcal{O}(\xi^0). \quad (23)$$

Thus, the calculation of the NTS term at tree-level remains straightforward as we just need to also calculate the derivatives w.r.t. the polarisation vector.

To extend this discussion to the one-loop level, we use the method of regions [53]. It was shown in [49], that the amplitude of the soft contribution is

$$\mathcal{A}_{n+1}^{(1), \text{soft}} = - \sum_{i \neq j} Q_i^2 Q_j^2 (i \mathcal{A}_n^{(0)}) \left(\frac{p_i \cdot \epsilon}{k \cdot p_i} - \frac{p_j \cdot \epsilon}{k \cdot p_j} \right) S(p_i, p_j, k) + \mathcal{O}(\xi^1). \quad (24)$$

The function $S(p_i, p_j, k) \sim k$ can be calculated universally and is presented in [49]. The hard contribution is closely related to the LBK theorem (23) with one important subtlety related to the following external leg corrections [50]

$$\mathcal{A}_{\text{ext},i}^{(1)} = p_i \text{Diagram with } \Gamma^{\text{ext}} \text{ and } p_\gamma \text{ on external leg } i \text{ (wavy)} + p_i \text{Diagram with } \Gamma^{\text{ext}} \text{ and } p_\gamma \text{ on external leg } i \text{ (wavy)} + p_i \text{Diagram with } \delta m \text{ and } \Gamma^{\text{ext}} \text{ and } p_\gamma \text{ on external leg } i \text{ (wavy)}. \quad (25)$$

The vertex correction to the soft photon emission spoils the basic assumption of the LBK theorem that diagrams with internal emission do not contain any $1/p_\gamma$ poles. Further, the self-energy correction is technically an external correction and could be expanded using the normal LBK theorem. Hence, these contributions do not reduce to the non-radiative amplitude. Instead, one can show that (25) results in an extra contribution of the form

$$\mathcal{A}_{\text{ext},i}^{(1)} = Q_i^3 \Gamma^{\text{ext}} \epsilon \cdot H u(p_i) \quad (26)$$

$$H_\mu = \frac{1}{m_i} \gamma^\mu - \frac{p_i^\mu}{m_i(k \cdot p_i)} \not{k} - \frac{1}{k \cdot p_i} \gamma^\mu \not{k}. \quad (27)$$

When interfering this contribution with the LP term of (19) we find

$$\mathcal{M}_{\text{ext},i}^{(1)} = \frac{1}{\xi} \sum_j Q_j \frac{\epsilon^* \cdot p_j}{k \cdot p_j} \Gamma^{\text{ext}} \epsilon \cdot H u(p_i) \bar{u}(p_i) \Gamma^{\text{ext},\dagger} + \text{h.c.} \quad (28)$$

In the unpolarised case, this contribution vanishes after some Dirac algebra. However, if $n_i \neq 0$, it does not and instead results in

$$\mathcal{M}_{\text{ext},i}^{(1)} = -\frac{1}{\xi} \sum_j \frac{Q_i^3 Q_j}{16\pi^2} \frac{1}{(k \cdot p_i)(k \cdot p_j)} \left[(2n \cdot p_j) k^\mu - (2n \cdot k) p_j^\mu \right] \left[\frac{\partial}{\partial n_{i,\mu}} \mathcal{M}_n^{(0)} - \frac{p_i^\mu}{m_i} \mathcal{M}_n^{(0),\prime} \right]. \quad (29)$$

Here, we need a modified version of the tree-level matrix element

$$\mathcal{M}_n^{(0),\prime} = \Gamma^{\text{ext}} (\not{p}_i + m_i) \gamma^5 \Gamma^{\text{ext},\dagger}. \quad (30)$$

We can now write down a version of the LBK theorem that is valid both at one-loop and in the case of polarised external particles

$$\begin{aligned} \mathcal{M}_{n+1}^{(1)} = \sum_{i,j} Q_i Q_j \left\{ -\frac{1}{\xi^2} \frac{p_i \cdot p_j}{(p_i \cdot k)(p_j \cdot k)} \mathcal{M}_n^{(1)} + \frac{1}{\xi} \frac{p_j \cdot D_i[\mathcal{M}_n^{(1)}]}{k \cdot p_j} \right. \\ \left. + \frac{1}{\xi} \frac{p_j^\mu (k \cdot n_i) - k_\mu (p_j \cdot n_i)}{(p_i \cdot k)(p_j \cdot k)} \left[\frac{\partial}{\partial n_{i,\mu}} \mathcal{M}_n^{(1)} + \frac{Q_i^2}{8\pi^2} \left(\frac{\partial}{\partial n_{i,\mu}} \mathcal{M}_n^{(0)} - \frac{p_i^\mu}{m_i} \mathcal{M}_n^{(0),\prime} \right) \right] \right\} \\ + \frac{1}{\xi} \sum_{l,i \neq j} Q_i^2 Q_j Q_l \left[\frac{p_i \cdot p_l}{(p_i \cdot k)(p_l \cdot k)} - \frac{p_l \cdot p_j}{(p_l \cdot k)(p_j \cdot k)} \right] \times 2 \mathcal{S}(p_i, p_j, k) \mathcal{M}_n^{(0)} + \mathcal{O}(\xi^0). \end{aligned} \quad (31)$$

The new term $\mathcal{M}_n^{(0),\prime}$, while easy to calculate, has severe consequences for the structure of the NTS approximation. Every other term in (31) is *directly* related to the reduced process, either at one-loop ($\mathcal{M}_n^{(1)}$) or tree-level ($\mathcal{M}_n^{(0)}$). $\mathcal{M}_n^{(0),\prime}$, on the other hand, is a new structure that spoils the elegance of the LBK theorem and its extensions.

We have numerically verified that (31) is correct by taking the limit $\xi \rightarrow 0$ of the real-virtual matrix element relevant for this process (as shown in Figure 1) and also for $\mu \rightarrow \nu \bar{\nu} e \gamma$.

4 Results

To validate our calculation, we have crossed it to $e\mu \rightarrow e\mu$ and compared the NLO-EW with [21] and the NNLO-QED with [22, 23] at the level of the differential distributions. We found full agreement in both cases.

In the following, we present some results for $e^+e^- \rightarrow \tau^+\tau^-$ at $\sqrt{s} = 10.5830052 \text{ GeV}$ both without any cuts and tailored to Belle II. We stress that these are just examples and that MCMULE can calculate any IR-safe observable.

We write the total EW cross section as

$$\sigma = \sigma_{\text{QED}} + \sigma_{\text{EW}} = \sigma_{\text{QED}}^{(0)} + \sigma_{\text{QED}}^{(1)} + \sigma_{\text{QED}}^{(2)} + \sigma_{\text{EW}}, \quad (32)$$

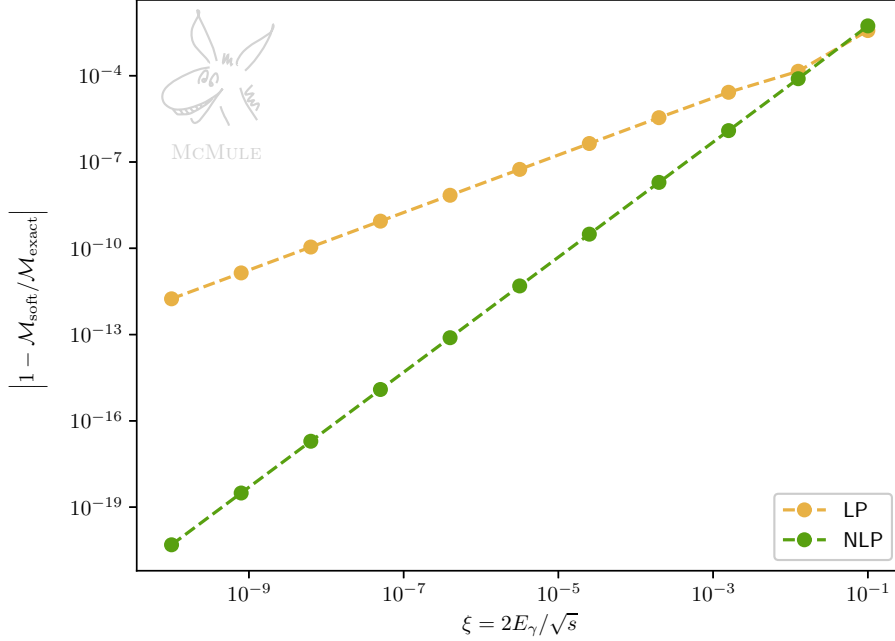


Figure 1: Convergence of the soft limit at LP and NLP of the dominant one-loop corrections to $e^+e^- \rightarrow \ell^+\ell^-\gamma$. The reference value $\mathcal{M}_{\text{exact}}$ is calculated with arbitrary precision in Mathematica.

which is divided into the pure QED and the EW part. The former are further split into LO ($\sigma_{\text{QED}}^{(0)}$), NLO ($\sigma_{\text{QED}}^{(1)}$), and NNLO ($\sigma_{\text{QED}}^{(2)}$) contributions. Note that we do not split $\sigma_{\text{EW}} \equiv \sigma_{\text{EW}}^{(0)} + \sigma_{\text{EW}}^{(1)}$ as they turn out to be similar in size. This is *not* a problem since we only expect perturbative convergence for the total EW cross section, i.e. $\sigma_{\text{QED}}^{(1)} + \sigma_{\text{EW}}^{(1)} \ll \sigma_{\text{QED}}^{(0)} + \sigma_{\text{EW}}^{(0)}$.

In the interest of Open Science, all raw data, analysis pipelines, and plots can be found at [54]

<https://mule-tools.gitlab.io/user-library/dilepton/belle>

4.1 Cross section without cuts

We begin by considering the cross section integrated over all of phase space without any cuts. The relevant K factors are defined as

$$\delta K^{(1)} = \frac{\sigma_{\text{QED}}^{(1)}}{\sigma_{\text{QED}}^{(0)}}, \quad \delta K^{(2)} = \frac{\sigma_{\text{QED}}^{(2)}}{\sigma_{\text{QED}}^{(0)} + \sigma_{\text{QED}}^{(1)}} \quad \text{and} \quad \delta K_{\text{EW}} = \frac{\sigma_{\text{EW}}}{\sigma_{\text{QED}}}. \quad (33)$$

We further consider the forward-backward asymmetry in the CMS frame which we denote with a *

$$A_{\text{FB}}(\sigma) = \frac{\int_0^{\pi/2} d\theta_{\tau^-}^* \frac{d\sigma}{d\theta_{\tau^-}^*} - \int_{\pi/2}^{\pi} d\theta_{\tau^-}^* \frac{d\sigma}{d\theta_{\tau^-}^*}}{\int_0^{\pi/2} d\theta_{\tau^-}^* \frac{d\sigma}{d\theta_{\tau^-}^*} + \int_{\pi/2}^{\pi} d\theta_{\tau^-}^* \frac{d\sigma}{d\theta_{\tau^-}^*}}. \quad (34)$$

The angles θ_{τ^\pm} are defined w.r.t. the incoming positron. At a given order, A_{FB} is defined to also contain all contributions below it, i.e.

$$A_{\text{FB}}(\sigma_{\text{QED}}^{(\ell)}) \equiv A_{\text{FB}}\left(\sum_{j=0}^{\ell} \sigma_{\text{QED}}^{(j)}\right), \quad A_{\text{FB}}(\sigma_{\text{EW}}) \equiv A_{\text{FB}}(\sigma_{\text{QED}} + \sigma_{\text{EW}}). \quad (35)$$

polarisation (00)					
	$\sigma_{\text{QED}}^{(0)}$	$\sigma_{\text{QED}}^{(1)}$	$\sigma_{\text{QED}}^{(2)}$	σ_{EW}	
σ / pb	771.640	139.286	4.158	0.140	
$\delta K / \%$		18.051	0.457	0.015	
A_{FB}	0	-0.012	n/a	-0.006	
polarisation ($\pm\pm$)					
	$\sigma_{\text{QED}}^{(0)}$	$\sigma_{\text{QED}}^{(1)}$	$\sigma_{\text{QED}}^{(2)}$	$\sigma_{\text{EW}}(++)$	$\sigma_{\text{EW}}(--)$
σ / pb	393.537	72.922	2.537(3)	0.007	
$\delta K / \%$		18.530	0.544	0.001	
A_{FB}	0	-0.012	n/a	-0.006	
polarisation ($\mp\pm$)					
	$\sigma_{\text{QED}}^{(0)}$	$\sigma_{\text{QED}}^{(1)}$	$\sigma_{\text{QED}}^{(2)}$	$\sigma_{\text{EW}}(-+)$	$\sigma_{\text{EW}}(+-)$
σ / pb	1149.744	205.648	5.782(1)	0.093	0.455
$\delta K / \%$		17.886	0.427	0.007	0.033
A_{FB}	0	-0.012	n/a	-0.006	-0.006

Table 1: Cross sections and asymmetries for $e^+e^- \rightarrow \tau^+\tau^-$ up to NNLO in QED and NLO in EW for all polarisation configurations (e^+e^-). When the electrons are polarised, the degree of polarisation is 70% in their respective rest frames. Unless otherwise indicated, all digits are significant.

The cross sections and asymmetries are shown in Table 1 for the unpolarised case and the cases where both electrons are polarised parallel (+) or anti-parallel (-) w.r.t. their direction of flight with a degree of polarisation of 70% in their rest frames. Note that in the QED case, parity invariance implies that there are only two independent configurations since

$$\sigma_{\text{QED}}(++) = \sigma_{\text{QED}}(--) \quad \text{and} \quad \sigma_{\text{QED}}(+-) = \sigma_{\text{QED}}(-+). \quad (36)$$

In the EW case, parity is violated but CP is still conserved. Hence,

$$\sigma_{\text{EW}}(+-) \neq \sigma_{\text{EW}}(-+) \quad \text{but} \quad \sigma_{\text{EW}}(++) = \sigma_{\text{EW}}(--), \quad (37)$$

implying three independent configurations.

The angular distributions used for A_{FB} are shown in Figure 2 for the unpolarised case. We note that even though the NNLO-QED and EW corrections are similar in size at the level of $d\sigma/d\theta^*$, the latter are much smaller for the integrated cross section. This is because the NNLO-QED corrections are symmetric while the EW corrections are antisymmetric as can be clearly seen in Figure 2. Note that the zero crossing of the EW corrections happens no longer at exactly 90° but is slightly offset due to the presence of radiative corrections.

At LO in QED, A_{FB} is exactly zero as expected, while at NLO in QED, the mixed tauonic-electronic contribution induces a finite but small asymmetry. This is similar to the NLO-QCD effects resulting in a non-zero A_{FB} for the hadronic $t\bar{t}$ production [55]. In principle, this would continue at NNLO in QED. However, the purely electronic contributions considered here are perfectly symmetric w.r.t. $\theta_{\tau^\pm}^*$ and therefore do not contribute to A_{FB} . The EW corrections are perfectly asymmetric but much smaller than the QED corrections. Hence, their asymmetry is drowned out by the QED part, resulting in a much lower asymmetry than naively expected.

4.2 Predictions for Belle II

Next, we tailor our calculation to Belle II. The detector is asymmetric since the electron beam's energy is higher than the positron beam's

$$E_{e^-}^{(\text{in})} = 7 \text{ GeV} \quad \text{and} \quad E_{e^+}^{(\text{in})} = 4 \text{ GeV}. \quad (38)$$

We approximate the detector's geometric acceptance by requiring that the tau leptons are produced within the geometric acceptance [56]

$$17^\circ < \theta_{\tau^\pm} < 150^\circ. \quad (39)$$

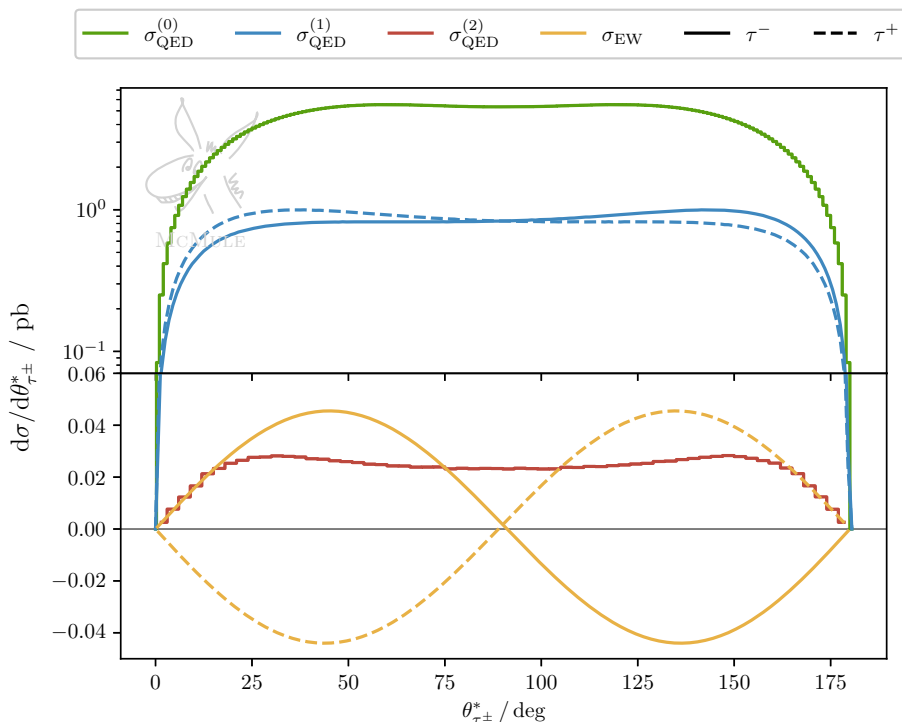


Figure 2: The angular distribution of the two taus in the final state for an unpolarised initial state in the CMS frame. Note that the scale changes from linear to logarithmic at +0.06.

The angular distribution of the outgoing taus is shown in Figure 3. The LO distribution vanishes below $\approx 53^\circ$ because of the cut on the other particle. However, once real emission is allowed, the angle can become much smaller. Once again, the EW corrections are similar in size to the NNLO-QED ones.

The SuperKEKB beams are currently unpolarised which is reflected in our calculation. However, recent proposals suggest that this could be changed in the future, aiming for 70% polarisation [57]. To study this case, we consider the ratio between the polarised and unpolarised angular distributions of the τ^- , both in the lab frame with cuts (θ_{τ^-}) and the CMS frame without ($\theta_{\tau^-}^*$)

$$\mathcal{R}^{(*)}(\pm+) = \frac{d\sigma(\pm+)/d\theta_{\tau^-}^{(*)}}{d\sigma(00)/d\theta_{\tau^-}^{(*)}} - \frac{\sigma(\pm+)}{\sigma(00)}. \quad (40)$$

Note that the first term in (40) is not centred around one but instead around $\sigma(\pm+)/\sigma(00)$. Hence, we subtract this overall shift to centre $\mathcal{R}(\pm+)$ around zero to make the comparison between $\mathcal{R}(++)$ and $\mathcal{R}(-+)$ easier.

\mathcal{R}^* and \mathcal{R} are shown in Figure 4. Let us first consider the simpler \mathcal{R}^* (Figure 4a). Since the outgoing taus are not polarised, $\mathcal{R}^* = 0$ at LO. At and beyond NLO, this is no longer true because hard-collinear ISR causes a helicity flip in the emitter.² With (40) normalised as it is, adding all polarisation results once again in a flat line, meaning that we have recovered the unpolarised result. Boosting to the lab frame (Figure 4b) stretches the distributions for forward emissions ($53^\circ \lesssim \theta_{\tau^-} \lesssim 120^\circ$) and squeezes them for backward ($120^\circ \lesssim \theta_{\tau^-} \lesssim 150^\circ$). Further, since the cuts (39) mean that hard emission is required for $\theta_{\tau^-} \lesssim 53^\circ$, the effect is significantly enhanced.

5 Conclusion

We have presented a fully differential calculation of the dominant NNLO-QED and NLO-EW corrections for di-lepton productions, including fermionic and bosonic corrections. We find that the EW corrections are

²We verified this with a dedicated run where we required that the initial-state emission is harder than $E_\gamma^* > 0.2 \text{ GeV}$ and $\cos \langle p_{e^-}^*, p_\gamma^* \rangle > 0.8$ in the CMS frame.

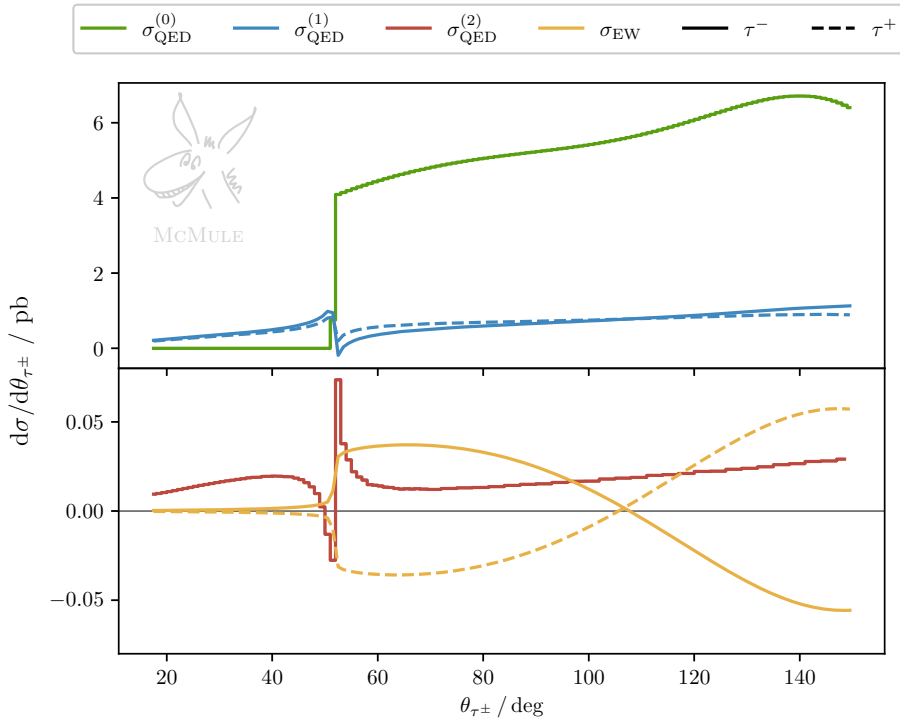


Figure 3: The angular distribution of the two taus in the lab frame for unpolarised initial states. Note that, because we only considered the dominant NNLO corrections, the $\sigma_{\text{QED}}^{(2)}$ curves for θ_{τ^+} and θ_{τ^-} are identical.

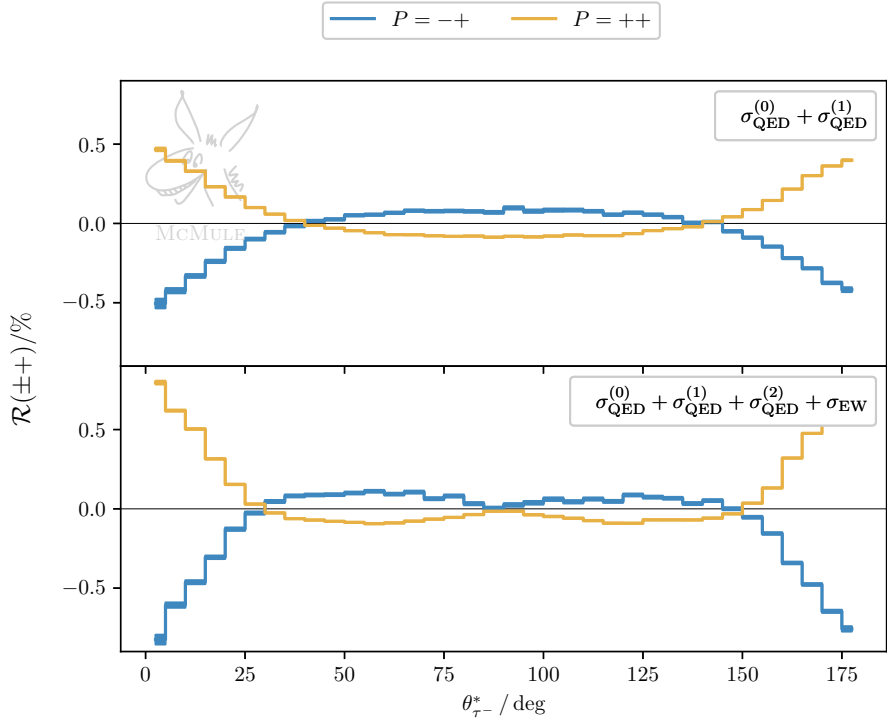
of similar size to the NNLO-QED ones for $\sqrt{s} \approx 10.5 \text{ GeV}$ meaning they are vital for Belle II. To perform this calculation, we have extended the strategy of next-to-soft stabilisation to polarised observables, which, combined with OpenLoops, allows for a fast and stable evaluation of the real-virtual matrix element.

All matrix elements were implemented in the parton-level Monte Carlo code MCMULE which allows the user to calculate arbitrary IR-safe observables. As a first example, we have calculated differential predictions for Belle II, both for polarised and unpolarised initial states.

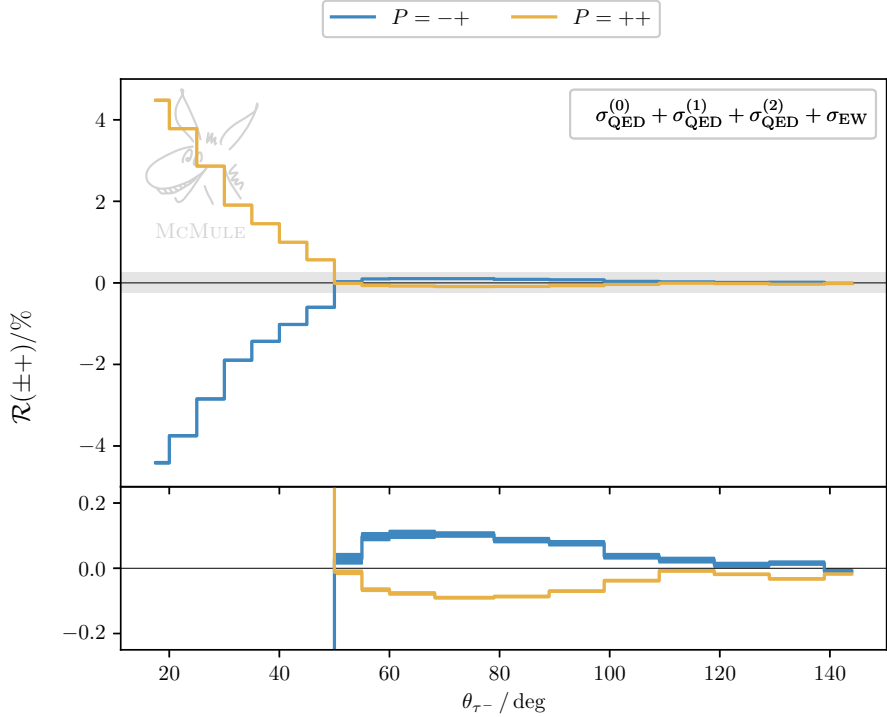
Since this calculation only includes the dominant contribution, a natural next step would be the inclusion of the full set of NNLO corrections, especially when considering asymmetries such as A_{FB} . The relevant two-loop matrix elements are known in the unpolarised case [16] but would need to be extended to the polarised case. Work to that end is currently in progress. Should even higher precision be required, further higher-order corrections could be efficiently approximated with a parton shower.

Acknowledgement

We are very grateful to our colleagues in the MCMULE collaboration, esp. Tim Engel, Franziska Hagelstein, Marco Rocco, and Adrian Signer, for supporting the implementation of this process, providing cross-checks, and comments to the manuscript. We would further like to thank Dominik Stöckinger and Fred Jegerlehner for useful discussion regarding the treatment of the EW-HVP corrections. We are also grateful to M. Zoller for providing the real-virtual matrix element in OpenLoops as well as for assisting us with its proper usage. Without the impressive numerical stability of OpenLoops this project would not have been possible. Finally, we would like to thank Peter Richardson and Lois Flower for useful discussions about the polarised distributions. YU acknowledges support by the UK Science and Technology Facilities Council (STFC) under grant ST/T001011/1. SK acknowledges partial support by the Swiss National Science Foundation (SNF) under grant 207386.



(a) \mathcal{R}^* in the CMS frame without cuts at NLO (upper panel) and for the full result (lower panel).



(b) \mathcal{R} in the lab frame with cuts for the full result. Note that the lower panel is zoomed in onto the θ_{τ^-} region that is allowed at tree-level.

Figure 4: The ratios $\mathcal{R}^{(*)}(++)$ in orange and $\mathcal{R}^{(*)}(-+)$ in blue, both in the CMS frame and in the lab frame. Note that this observable is very insensitive to EW effects and that the shape of the plots originates from the QED corrections. This means that we only need to show two out of the four different polarisation configurations.

References

- [1] BELLE-II collaboration, W. Altmannshofer et al., *The Belle II Physics Book*, *PTEP* **2019** (2019) 123C01 [[1808.10567](#)].
- [2] BELLE collaboration, J. Sasaki, *Study of tau five-body leptonic decays at Belle*, *Nucl. Part. Phys. Proc.* **287-288** (2017) 212.
- [3] BABAR collaboration, B. Oberhof, *Measurement of the branching fractions of radiative leptonic τ decays $\tau \rightarrow \ell\gamma\nu\bar{\nu}$, ($\ell = e, \mu$) at BaBar*, *Nucl. Part. Phys. Proc.* **260** (2015) 12 [[1502.01810](#)].
- [4] Y.-S. Tsai, *Decay Correlations of Heavy Leptons in $e^+e^- \rightarrow \ell^+\ell^-$* , *Phys. Rev. D* **4** (1971) 2821.
- [5] A. Crivellin, M. Hoferichter and J. M. Roney, *Towards testing the magnetic moment of the tau at one part per million*, [2111.10378](#).
- [6] S. Jadach, B. F. L. Ward and Z. Was, *Coherent exclusive exponentiation for precision Monte Carlo calculations*, *Phys. Rev. D* **63** (2001) 113009 [[hep-ph/0006359](#)].
- [7] S. Jadach, B. F. L. Ward and Z. Was, *The Precision Monte Carlo event generator KK for two fermion final states in e^+e^- collisions*, *Comput. Phys. Commun.* **130** (2000) 260 [[hep-ph/9912214](#)].
- [8] A. Arbuzov, S. Jadach, Z. Was, B. F. L. Ward and S. A. Yost, *The Monte Carlo Program KKMC, for the Lepton or Quark Pair Production at LEP/SLC Energies—Updates of electroweak calculations*, *Comput. Phys. Commun.* **260** (2021) 107734 [[2007.07964](#)].
- [9] A. Arbuzov, S. Bondarenko, Y. Dydyshka, L. Kalinovskaya, L. Rumyantsev, R. Sadykov et al., *Effects of electroweak radiative corrections in polarized low-energy electron-positron annihilation into lepton pairs*, [2206.09469](#).
- [10] P. Banerjee et al., *Theory for muon-electron scattering @ 10 ppm: A report of the MUonE theory initiative*, *Eur. Phys. J. C* **80** (2020) 591 [[2004.13663](#)].
- [11] C. M. Carloni Calame, M. Passera, L. Trentadue and G. Venanzoni, *A new approach to evaluate the leading hadronic corrections to the muon $g - 2$* , *Phys. Lett. B* **746** (2015) 325 [[1504.02228](#)].
- [12] G. Abbiendi et al., *Measuring the leading hadronic contribution to the muon $g - 2$ via μe scattering*, *Eur. Phys. J. C* **77** (2017) 139 [[1609.08987](#)].
- [13] C. Matteuzzi, G. Venanzoni, D. Abbaneo, G. Abbiendi, G. Bagliesi, D. Banerjee et al., *Letter of Intent: the MUonE project*, Tech. Rep. CERN-SPSC-2019-026. SPSC-I-252, CERN, Geneva, Jun, 2019.
- [14] P. Mastrolia, M. Passera, A. Primo and U. Schubert, *Master integrals for the NNLO virtual corrections to μe scattering in QED: the planar graphs*, *JHEP* **11** (2017) 198 [[1709.07435](#)].
- [15] S. Di Vita, S. Laporta, P. Mastrolia, A. Primo and U. Schubert, *Master integrals for the NNLO virtual corrections to μe scattering in QED: the non-planar graphs*, *JHEP* **09** (2018) 016 [[1806.08241](#)].
- [16] R. Bonciani et al., *Two-Loop Four-Fermion Scattering Amplitude in QED*, *Phys. Rev. Lett.* **128** (2022) 022002 [[2106.13179](#)].
- [17] A. A. Penin, *Two-loop photonic corrections to massive Bhabha scattering*, *Nucl. Phys. B* **734** (2006) 185 [[hep-ph/0508127](#)].
- [18] A. Mitov and S. Moch, *The Singular behavior of massive QCD amplitudes*, *JHEP* **05** (2007) 001 [[hep-ph/0612149](#)].
- [19] T. Becher and K. Melnikov, *Two-loop QED corrections to Bhabha scattering*, *JHEP* **06** (2007) 084 [[0704.3582](#)].

- [20] T. Engel, C. Gnendiger, A. Signer and Y. Ulrich, *Small-mass effects in heavy-to-light form factors*, *JHEP* **02** (2019) 118 [[1811.06461](#)].
- [21] M. Alacevich, C. M. Carloni Calame, M. Chiesa, G. Montagna, O. Nicrosini and F. Piccinini, *Muon-electron scattering at NLO*, *JHEP* **02** (2019) 155 [[1811.06743](#)].
- [22] P. Banerjee, T. Engel, A. Signer and Y. Ulrich, *QED at NNLO with McMule*, *SciPost Phys.* **9** (2020) 027 [[2007.01654](#)].
- [23] C. M. Carloni Calame, M. Chiesa, S. M. Hasan, G. Montagna, O. Nicrosini and F. Piccinini, *Towards muon-electron scattering at NNLO*, *JHEP* **11** (2020) 028 [[2007.01586](#)].
- [24] P. Banerjee, T. Engel, N. Schalch, A. Signer and Y. Ulrich, *Bhabha scattering at NNLO with next-to-soft stabilisation*, *Phys. Lett. B* **820** (2021) 136547 [[2106.07469](#)].
- [25] T. Hahn, *Generating Feynman diagrams and amplitudes with FeynArts 3*, *Comput. Phys. Commun.* **140** (2001) 418 [[hep-ph/0012260](#)].
- [26] P. Nogueira, *Automatic Feynman graph generation*, *J.Comput.Phys.* **105** (1993) 279.
- [27] H. H. Patel, *Package-X: A Mathematica package for the analytic calculation of one-loop integrals*, *Comput. Phys. Commun.* **197** (2015) 276 [[1503.01469](#)].
- [28] D. A. Ross and J. C. Taylor, *Renormalization of a unified theory of weak and electromagnetic interactions*, *Nucl. Phys. B* **51** (1973) 125.
- [29] A. Denner, *Techniques for calculation of electroweak radiative corrections at the one loop level and results for W physics at LEP-200*, *Fortsch. Phys.* **41** (1993) 307 [[0709.1075](#)].
- [30] Y. Ulrich, *MCMULE: QED Corrections for Low-Energy Experiments*, Ph.D. thesis, University of Zurich, 2020. [2008.09383](#).
- [31] Y. Ulrich et al., *The MCMULE Manual*, [doi:10.5281/zenodo.6046769](#) [[mule-tools.gitlab.io/manual](#)].
- [32] T. Engel, A. Signer and Y. Ulrich, *A subtraction scheme for massive QED*, *JHEP* **01** (2020) 085 [[1909.10244](#)].
- [33] S. Frixione, Z. Kunszt and A. Signer, *Three jet cross-sections to next-to-leading order*, *Nucl. Phys. B* **467** (1996) 399 [[hep-ph/9512328](#)].
- [34] R. Frederix, S. Frixione, F. Maltoni and T. Stelzer, *Automation of next-to-leading order computations in QCD: The FKS subtraction*, *JHEP* **10** (2009) 003 [[0908.4272](#)].
- [35] G. Moortgat-Pick et al., *The Role of polarized positrons and electrons in revealing fundamental interactions at the linear collider*, *Phys. Rept.* **460** (2008) 131 [[hep-ph/0507011](#)].
- [36] H. E. Haber, *Spin formalism and applications to new physics searches*, in *21st Annual SLAC Summer Institute on Particle Physics: Spin Structure in High-energy Processes (School: 26 Jul - 3 Aug, Topical Conference: 4-6 Aug) (SSI 93)*, pp. 231–272, 4, 1994, [hep-ph/9405376](#).
- [37] F. Buccioni, S. Pozzorini and M. Zoller, *On-the-fly reduction of open loops*, *Eur. Phys. J. C* **78** (2018) 70 [[1710.11452](#)].
- [38] F. Buccioni, J.-N. Lang, J. M. Lindert, P. Maierhöfer, S. Pozzorini, H. Zhang et al., *OpenLoops 2*, *Eur. Phys. J. C* **79** (2019) 866 [[1907.13071](#)].
- [39] F. Jegerlehner, *Renormalizing the standard model*, *Conf. Proc. C* **900603** (1990) 476.
- [40] F. Jegerlehner, *Variations on Photon Vacuum Polarization*, *EPJ Web Conf.* **218** (2019) 01003 [[1711.06089](#)].
- [41] M. J. Levine and R. Roskies, *Hyperspherical approach to quantum electrodynamics - sixth-order magnetic moment*, *Phys. Rev. D* **9** (1974) 421.

- [42] M. J. Levine, R. C. Perisho and R. Roskies, *Analytic contributions to the g factor of the electron*, *Phys. Rev. D* **13** (1976) 997.
- [43] M. Fael, *Hadronic corrections to μ - e scattering at NNLO with space-like data*, *JHEP* **02** (2019) 027 [[1808.08233](#)].
- [44] P. Banerjee, T. Engel, N. Schalch, A. Signer and Y. Ulrich, *Møller scattering at NNLO*, *Phys. Rev. D* **105** (2022) L031904 [[2107.12311](#)].
- [45] W. Bernreuther, R. Bonciani, T. Gehrmann, R. Heinesch, T. Leineweber, P. Mastrolia et al., *Two-loop QCD corrections to the heavy quark form-factors: The Vector contributions*, *Nucl. Phys. B* **706** (2005) 245 [[hep-ph/0406046](#)].
- [46] E. Remiddi and J. A. M. Vermaseren, *Harmonic polylogarithms*, *Int. J. Mod. Phys. A* **15** (2000) 725 [[hep-ph/9905237](#)].
- [47] F. E. Low, *Bremsstrahlung of very low-energy quanta in elementary particle collisions*, *Phys. Rev.* **110** (1958) 974.
- [48] T. H. Burnett and N. M. Kroll, *Extension of the low soft photon theorem*, *Phys. Rev. Lett.* **20** (1968) 86.
- [49] T. Engel, A. Signer and Y. Ulrich, *Universal structure of radiative QED amplitudes at one loop*, *JHEP* **04** (2022) 097 [[2112.07570](#)].
- [50] T. Engel, *Muon-Electron Scattering at NNLO*, Ph.D. thesis, University of Zurich, 2022. [2209.11110](#).
- [51] A. V. Tarasov, *Observables in the bremsstrahlung in the low approximation.*, *Yad. Fiz.* **8** (1968) 1191.
- [52] H. W. Fearing, *Note on the generalization of the burnett-kroll soft-photon theorem to polarized cross-sections*, *Phys. Rev. D* **7** (1973) 243.
- [53] M. Beneke and V. A. Smirnov, *Asymptotic expansion of Feynman integrals near threshold*, *Nucl. Phys. B* **522** (1998) 321 [[hep-ph/9711391](#)].
- [54] Y. Ulrich et al., *The MCMULE Dataset*, [doi:10.5281/zenodo.6541686](#) [[mule-tools.gitlab.io/user-library](#)].
- [55] J. H. Kühn and G. Rodrigo, *Charge asymmetry of heavy quarks at hadron colliders*, *Phys. Rev. D* **59** (1999) 054017 [[hep-ph/9807420](#)].
- [56] BELLE collaboration, A. Abashian et al., *The Belle Detector*, *Nucl. Instrum. Meth. A* **479** (2002) 117.
- [57] US BELLE II GROUP, BELLE II/SUPERKEKB e^- POLARIZATION UPGRADE WORKING GROUP collaboration, D. M. Asner et al., *Snowmass 2021 White Paper on Upgrading SuperKEKB with a Polarized Electron Beam: Discovery Potential and Proposed Implementation*, in *2022 Snowmass Summer Study*, 5, 2022, [2205.12847](#).